May 1, 2007

Recent Astronomical Commissioning Results for the Ka-band (26.0-40 GHz) Receiver

D.J. Pisano, Ron Maddalena, Charles Figura, Jeff Wagg

ABSTRACT

We present an observing procedure and calibration algorithm for use with the refurbished Ka-band (26-40 GHz) receiver on the GBT. This method yields flat baselines and noise that integrates down as theoretically expected. We present the derived T_{cal} and T_{sys} values for both feeds and both polarizations of the receiver. We used these procedures to successfully detect redshifted CO emission at $z = 2.3$ for the first time with the Ka-band receiver.

1. Background

During the summer of 2006, the Ka-band receiver underwent a major renovation to alleviate critical problems with intermittent, irregular baseline structures. These structures prevented the noise from integrating down as theoretically expected. The baseline structure had a periodicity of 10-50 MHz, frustrating attempts to observe wide spectral lines. The status of the receiver through August 2006 is summarized in various documents available elsewhere [1].

The Ka-band receiver was designed as a correlation receiver containing a pair of hybrids/phase-switches for use with the Caltech Continuum Backend (CCB) and the Zpectrometer. The phase-switches can rapidly switch between independent combinations of feeds and polarization. It was hoped that this rapid switching, in concert with the engineering improvements to the receiver, would eliminate the gain variations causing the spectral baseline structure. Unfortunately, while successful observations have been conducted with the CCB, there were still problems with Zpectrometer observations and standard Spectrometer observations. It has been difficult to detect broad emission lines (a few hundred km/s) from known sources (such as highly-redshifted CO lines), and impossible to conduct blind searches for such broad lines when the line frequency is uncertain. As a result, during the 2006-2007 high-frequency observing season only continuum observations and narrow-line spectroscopy projects were scheduled.

In this memo, we present an observing procedure and calibration algorithm resulting in flat baselines sufficient for observations of broad-line sources with the Ka-band receiver and the GBT

[1] *http://wiki.gb.nrao.edu/bin/view/Projects/SpectralBaselines*

Spectrometer. This algorithm involves using the Ka-band receiver as a total power receiver and does not utilize the full capabilities of the correlation receiver design. In Section 2 we present the mathematical basis for our calibration algorithm. Section 3 details our on-sky tests of various observing modes using this calibration algorithm. We present measurements of the calibration and system temperatures in Section 4. The first detection of a redshifted CO line with the Ka-band receiver is presented in Section 5, while outstanding issues and future work are discussed in Section 6.

2. Calibration Routines

2.1. Ka-band Signal Path

Figure 1 summarizes the salient parts of the Ka-band receiver hardware for this memo. The receiver has dual beams (labeled 1 and 2) and dual polarizations (L and R). The combination of feed and polarization are labeled L1, L2, R1, and R2. There are four output IF's, labeled for our purposes as A, B, C, and D. Each IF feeds a Spectrometer sampler (similarly labeled A, B, C, and D). There are two pairs of switchable hybrids, upper (U) and lower (L); the low noise amplifiers are located between the hybrids in each pair. The two inputs to each hybrid are of opposite polarization and come from different feeds; they can be switched by the Spectrometer. If the Spectrometer sets its switching signal to 'Sig', then IFA will be connected to R1 and IFB to L2. If the Spectrometer sets the switching signal to 'Ref', then IFA will be connected to L2 and IFB to R1. *Note that 'Sig' and 'Ref' refer to the sense of a TTL*[2] *signal and is a misnomer with regards to whether the data are taken towards a source or towards blank sky.* The Spectrometer can also cycle the noise diode 'On' and 'Off'. Through the control software, one can specify whether the L, R, or both diodes are to be fired.

2.2. Calibration Algorithms

Typically, observation procedures consist of a 'nod' observation where the source is first positioned in front of feed 1. Then, the telescope is moved (i.e., standard nodding) or the subreflector is tilted (subreflector nodding, an experimental observing mode) such that the source is placed in front of feed 2. We will label the two halves of the nod as 'Pos1' and 'Pos2'

In all, there are 32 'spectra' that the Spectrometer collects for each observation – two positions of the 'nod', two feeds, two polarizations, 'Sig' and 'Ref' switching states, diode 'On' and 'Off'. Each Spectrometer sampler collects 8 spectra. With such a plethora of spectra, there are multiple ways in which the data can be combined; finding the algorithm that produces the best baselines is

[2]transistor-transistor logic

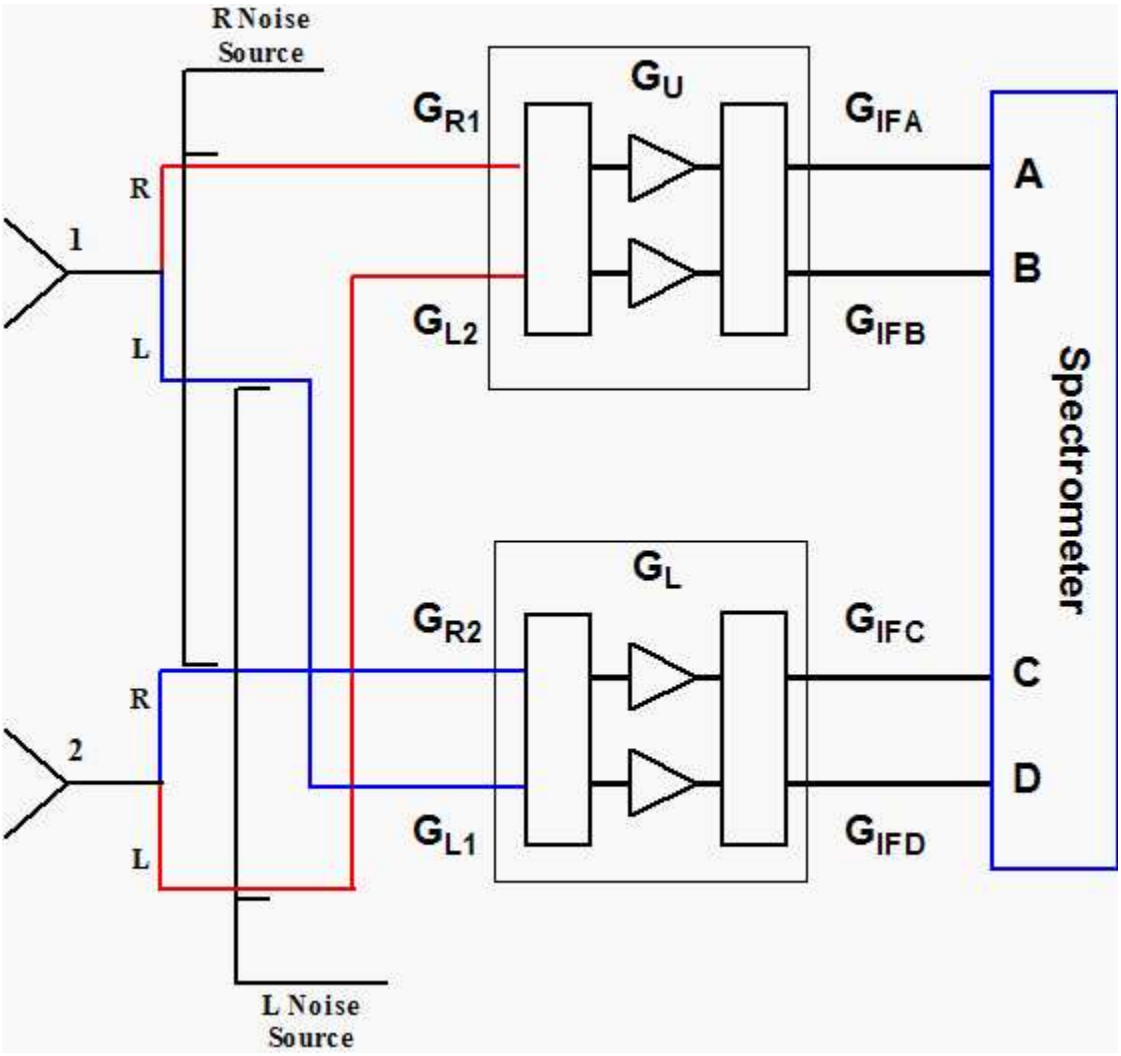

Fig. 1.— Schematic of Ka-Band receiver and signal path.

a challenge.

Figure 1 summarizes the various sources of gain in the signal path. We assume the gains are not necessarily equal in front of the hybrids (G_{L1}, G_{R1}, G_{L2}, and G_{R2}) or after the hybrids (G_{IFA}, G_{IFB}, G_{IFC}, G_{IFD}). Since the hybrids combine their input signals, the two signals passing through a hybrid see the same gain (either G_U or G_L) although the gain of each hybrid is different.

We will use the 8 spectra collected by sampler 'A' to illustrate the calibration procedure.

$$\begin{aligned}
V_{pos1_sig_off_A} &= \left(T_{src} + T_{atm} + T_{Rx}^{R1}\right) \cdot G_{R1} G_U G_{IFA} \\
V_{pos1_sig_on_A} &= \left(T_{src} + T_{atm} + T_{Rx}^{R1} + T_{cal}^{R1}\right) \cdot G_{R1} G_U G_{IFA} \\
V_{pos1_ref_off_A} &= \left(T_{atm} + T_{Rx}^{L2}\right) \cdot G_{L2} G_U G_{IFA} \\
V_{pos1_ref_on_A} &= \left(T_{atm} + T_{Rx}^{L2} + T_{cal}^{L2}\right) \cdot G_{L2} G_U G_{IFA} \\
V_{pos2_sig_off_A} &= \left(T_{atm} + T_{Rx}^{R1}\right) \cdot G_{R1} G_U G_{IFA} \\
V_{pos2_sig_on_A} &= \left(T_{atm} + T_{Rx}^{R1} + T_{cal}^{R1}\right) \cdot G_{R1} G_U G_{IFA} \\
V_{pos2_ref_off_A} &= \left(T_{src} + T_{atm} + T_{Rx}^{L2}\right) \cdot G_{L2} G_U G_{IFA} \\
V_{pos2_ref_on_A} &= \left(T_{src} + T_{atm} + T_{Rx}^{L2} + T_{cal}^{L2}\right) \cdot G_{L2} G_U G_{IFA}
\end{aligned} \tag{1}$$

In Equation 1, T_{src} is the source intensity that we are trying to measure; T_{atm} represents the contribution from the atmosphere plus any signal that is coming into the feed (spillover, CMB) except the signal from the source. T_{atm} is assumed to vary smoothly with frequency, if at all, and is identical in all signal paths. T_{Rx} represents anything that has significant frequency structure, like the classical definition of receiver's temperature, and may be different in the various signal paths. Although various components in the signal path can contribute to T_{Rx}, we're modeling T_{Rx} as if it were coming into the feed, a simplifying assumption that is of no consequence to this discussion. In our model, there are no temporal changes in T_{Rx} since such changes can be represented as a change in gain. T_{cal} represents the noise diode's contribution, which we will assume has a significant frequency structure but is temporally stable. Although there are only two diodes (L and R), there are different diode couplers for each polarization and feed – therefore, we do not assume the diode signal injected into, say, L1 is the same as is injected into L2. We discuss in Sections 2.3 and 3.4 the effects of spatial or temporal variations in gain or T_{atm}.

Throughout, we'll be using the following averages:

$$\begin{aligned}
V_{pos1_sig_A} &= (V_{pos1_sig_on_A} + V_{pos1_sig_off_A})/2 \\
V_{pos2_sig_A} &= (V_{pos2_sig_on_A} + V_{pos2_sig_off_A})/2 \\
V_{sig_on_A} &= (V_{pos1_sig_on_A} + V_{pos2_sig_on_A})/2 \\
V_{sig_off_A} &= (V_{pos1_sig_off_A} + V_{pos2_sig_off_A})/2
\end{aligned} \tag{2}$$

with similar equations for 'Ref' and the B, C, and D samplers.

It is tempting to use a calibration algorithm that would be appropriate for a true beam-switched receiver and that would difference the spectra taken with the hybrid in its 'Sig' and 'Ref'

states. One such algorithm would include terms like:

$$T_a = \frac{1}{2}\left[\frac{V_{pos1\_sig\_A} - V_{pos1\_ref\_A}}{V_{pos1\_sig\_on\_A} - V_{pos1\_sig\_off\_A}} \cdot T_{cal}^{R1} + \frac{V_{pos2\_ref\_A} - V_{pos2\_sig\_A}}{V_{pos2\_ref\_on\_A} - V_{pos2\_ref\_off\_A}} \cdot T_{cal}^{L2}\right] \quad (3)$$

plus three similar equations for the remaining samplers. Substituting the definitions of Equations 1 and 2 into Equation 3, and then averaging the four versions of Equation 3 for the various Spectrometer samplers produces the grand average of:

$$\begin{array}{l} T_a = T_{src} + T_{atm}\left(1 - \frac{G_{L2}}{4G_{R1}} - \frac{G_{R1}}{4G_{L2}} - \frac{G_{L1}}{4G_{R2}} - \frac{G_{R2}}{4G_{L1}}\right) \\ +\frac{1}{4}\left[\begin{array}{l} \left(T_{Rx}^{L2} + \frac{T_{cal}^{L2}}{2}\right)\left(1 - \frac{G_{L2}}{G_{R1}}\right) + \left(T_{Rx}^{R1} + \frac{T_{cal}^{R1}}{2}\right)\left(1 - \frac{G_{R1}}{G_{L2}}\right) \\ + \left(T_{Rx}^{L1} + \frac{T_{cal}^{L1}}{2}\right)\left(1 - \frac{G_{L1}}{G_{R2}}\right) + \left(T_{Rx}^{R2} + \frac{T_{cal}^{R2}}{2}\right)\left(1 - \frac{G_{R2}}{G_{L1}}\right) \end{array}\right] . \end{array} \quad (4)$$

Since the correct answer should be simply $T_a = T_{src}$, it is apparent that this algorithm has problems. It works only if the gains in front of the hybrid have equal magnitude (i.e. $G_{R1} = G_{L2}$, and $G_{L1} = G_{R2}$) and frequency structure. (Note that the T_{cal} terms could be eliminated if one were to use only those spectra with the noise diode off for the numerators in Equation 3. This will result in the loss of half of one's data.) We have yet to find an algorithm that can difference the 'Sig' and 'Ref' spectra and yields good baselines; all such algorithms seem to require perfectly matching gains in front of the hybrids.

The algorithm that has worked best for us is more akin to that used for wide-band observations with non-correlation receivers and is very similar to that presented by Hynes, Maddalena, and Figura[3] (2006, AAS, 209, 85.04). Here, we difference the Pos1 and Pos2 spectra for the same phase of the hybrid. The algorithm consists of terms like:

$$T_a = \frac{1}{2}\left[\frac{V_{pos1\_sig\_A} - V_{pos2\_sig\_A}}{V_{sig\_on\_A} - V_{sig\_off\_A}} \cdot T_{cal}^{R1} + \frac{V_{pos2\_ref\_A} - V_{pos1\_ref\_A}}{V_{ref\_on\_A} - V_{ref\_off\_A}} \cdot T_{cal}^{L2}\right] \quad (5)$$

with similar equations for the B, C, and D samplers. Substituting the above definitions for the various spectra produces T_a=T_{src}, our desired result. There is no need to make any assumptions about the receiver gains or to discard any data if both diodes are firing. If only one diode is firing, then improved baselines are still achievable by discarding data without the diode and dropping the second term in Equation 5.

For high resolution observations or observations with short duration, the denominators in Equation 5 can have a noise level that exceeds the mean value of the denominator. Equation 5 will then blow up since some channels will have a numerator value that is close to zero or negative.

[3]available at: http://www.gb.nrao.edu/ rmaddale/GBT/HighPrecisionCalibrationWithGBT.pdf

One could smooth the denominators using, for example, a Savitzky-Golay smoothing filter. If one takes the mean of the denominators over almost all of the channels, one would essentially be using the alternative algorithm of:

$$T_a = \frac{1}{2}\left[\frac{V_{pos1\_sig\_A} - V_{pos2\_sig\_A}}{V_{pos2\_sig\_A}} \cdot T_{sys}^{R1} + \frac{V_{pos2\_ref\_A} - V_{pos1\_ref\_A}}{V_{pos1\_ref\_A}} \cdot T_{sys}^{L2}\right] \quad (6)$$

This is the traditional $T_{sys} \times \frac{Source-Sky}{Sky}$ algorithm used by most radio telescopes.

The T_{cal} values in Equation 5 must have sufficient frequency resolution and be highly accurate. Some of the consequences of using T_{cal} that has insufficient frequency resolution include baseline shapes that will either be introduced or not properly alleviated, a noise in the spectrum that may improperly vary across the band, and incorrect line intensities. If two or more spectral line features are in the same bandpass, even the relative line intensities can be wrong. One can astronomically derive sufficiently accurate values for T_{cal} by observing flux calibrators and using the method outlined in Maddalena & Johnson[4] (2005, AAS, 207, 173.02) where one essentially inverts each term in Equation 5 to solve for T_{cal}.

Observers should be aware that data from a single sampler may not produce properly calibrated results. There is cross-talk between different paths through the hybrid that can be as high as -10 dB. For example, when the hybrid phase switch is in its 'Sig' position, sampler A in the Spectrometer should only see a signal that enters R1. With the cross-talk, however, sampler A may detect a signal that is 90% R1 and 10% L2. The situation would be reversed for sampler B. The noise in the data from samplers A and B will also be partially correlated. While the spectra from the samplers are individually corrupted, the average of the spectra from A and B will have the expected signal-to-noise since both the signal and noise are correlated between the samplers. Astronomically derived T_{cal} values must also be corrupted by the low isolation and probably don't completely represent the actual signal produced by the diodes. However, since the equations used to derive T_{cal} are inverted versions of those used to calibrate data any defect introduced into the calibration by the low isolation is canceled by the complimentary defect in the T_{cal} values.

2.3. Stability

Although Equation 5 produces the desired result, up to now we have been assuming that the gain and T_{atm} are identical between the Pos1 and Pos2 observations. In short, gain stability, rather than gain balancing, is most important for those using the Spectrometer with Ka-band. To see this, consider a change in gain and T_{atm} by redefining the Pos2 spectra in Equation 1:

[4]available at: http://www.gb.nrao.edu/ rmaddale/GBT/HighPrecisionCalibrationWithGBT.pdf

$$
\begin{aligned}
V_{pos2\_sig\_off\_A} &= \left(T_{atm} + \Delta T_{atm} + T_{Rx}^{R1}\right)\left(G_{R1} + \Delta G_{R1}\right)\left(G_U + \Delta G_U\right)\left(G_{IFA} + \Delta G_{IFA}\right) \\
V_{pos2\_sig\_on\_A} &= \left(T_{atm} + \Delta T_{atm} + T_{Rx}^{R1} + T_{cal}^{R1}\right)\left(G_{R1} + \Delta G_{R1}\right)\left(G_U + \Delta G_U\right)\left(G_{IFA} + \Delta G_{IFA}\right) \\
V_{pos2\_ref\_off\_A} &= \left(T_{src} + T_{atm} + \Delta T_{atm} + T_{Rx}^{L2}\right)\left(G_{L2} + \Delta G_{L2}\right)\left(G_U + \Delta G_U\right)\left(G_{IFA} + \Delta G_{IFA}\right) \\
V_{pos2\_ref\_on\_A} &= \left(T_{src} + T_{atm} + \Delta T_{atm} + T_{Rx}^{L2} + T_{cal}^{L2}\right)\left(G_{L2} + \Delta G_{L2}\right)\left(G_U + \Delta G_U\right)\left(G_{IFA} + \Delta G_{IFA}\right)
\end{aligned}
\tag{7}
$$

but retaining the definitions in Equation 1 for the Pos1 spectra. If we assume the deltas are small, and thus only keep first order terms, then Equation 5 for sampler A becomes:

$$
T_a = T_{src} + \frac{1}{2}\left[\begin{array}{l}
\left(\frac{\Delta G_{L2}}{G_{L2}} - \frac{\Delta G_{R1}}{G_{R1}}\right)\left(\frac{T_{src}+\Delta T_{atm}}{2} - T_{atm}\right) \\
+\left(\frac{\Delta G_U}{G_U} + \frac{\Delta G_{IFA}}{G_{IFA}}\right)\left(\frac{T_{cal}^{L2}-T_{cal}^{R1}}{2} + T_{Rx}^{L2} - T_{Rx}^{R1}\right) \\
+\frac{T_{cal}^{L2}\Delta G_{L2}}{2G_{L2}} - \frac{T_{cal}^{R1}\Delta G_{R1}}{2G_{R1}}
\end{array}\right]
\tag{8}
$$

with analogous equations for the B, C, and D samplers.

Note how a change in atmosphere is a second order affect since such a change introduces baseline shapes only if there is also a change in the gains before the hybrid. If one were to throw away the noise-diode 'on' data in the numerators of Equation 5, then the T_{cal} terms in Equation 8 drop out with a possible improvement in baseline shapes. Such a loss of integration time might be worthwhile if baselines are improved.

3. Observational Tests

We carried out a number of observational tests of the calibration algorithm presented in Section 2. Specifically, we compared the baseline shapes when:

- one diode is fired vs. two diodes,
- firing the hybrid phase-switches vs. leaving them in one state,
- rapidly nodding the subreflector (9 second cycles) vs. using the standard slow nods (2 minute cycles),
- short nodding cycle times vs. long cycle times.

We deal with each of these in turn below. For these tests, we use data taken either on the north celestial pole (NCP) on December 19, 2006 or on the high redshift galaxy IRAS FSC10214+4724 (F10214) on January 27, 2007 and April 7, 2007. All of the data have been reduced using Equation 5. Because of the problems with Equation 3 that have been demonstrated analytically, we did not test it with on-sky data.

3.1. Diodes

Our first comparison is between observations taken with just the L diode firing versus both the L and R diodes firing. In both cases, the hybrid phase-switch is firing and data from both states are combined. The data used are from tracks on the NCP, so the "nodding" is simulated by treating consecutive scans as separate positions. The results are shown in Figures 2 and 3.

Figure 2 represents the traditional observing mode of the Ka-band receiver. The prominent baseline structure is immediately visible. The noise in the spectrum is also much larger than that seen in Figure 3. It is clear from these figures that, *when the phase switches are active*, firing both diodes produces better noise and baseline shapes than only firing one diode. This is because the different gains do not cancel when only one diode is fired, but will when two diodes are active. This can be seen in Equation 5.

3.2. Phase-Switching

The second comparison is between using the phase switches (Figure 3) or leaving the phase switches in one state and treating the receiver as a total power receiver (Figure 4).

Both spectra have the same integration time, but the noise is about 12% higher in the total power spectrum than in the switched spectrum. Qualitatively, the baseline shapes are both equally flat. If we take the ratio of the noise over most of the band, 600 MHz, to just the central 50 MHz, we obtain a quantitative measure of the baseline shape that is independent of the integration time. In both cases, the ratio is about 1.15; the central portion of the spectrum is noisier than the outer portions. Since the noise is lower when the phase switches are active, this should be the preferred observing method.

It should be remembered that even when the phase switches are firing, we are not using the receiver as a correlation receiver. The data are reduced using Equation 5 whether the phase switches are active or not. Remember that if only the L diode is firing, then we can still recover the flat baselines by only looking at the L polarization data when the phase switches are active.

3.3. Nodding

As discussed in Section 2.2, the baseline structure is due to gain variations in the signal path. These variations are exacerbated when there is a significant difference between the source and sky temperatures. The can occur when observing a bright source or if the atmospheric opacity or temperature changes between the two positions of a nod. Standard nodding involves moving the entire telescope to switch the two Ka-band beams between the source and a neighboring sky position with typical cycle times of 2 minutes (one minute in each position). Cycle times as short

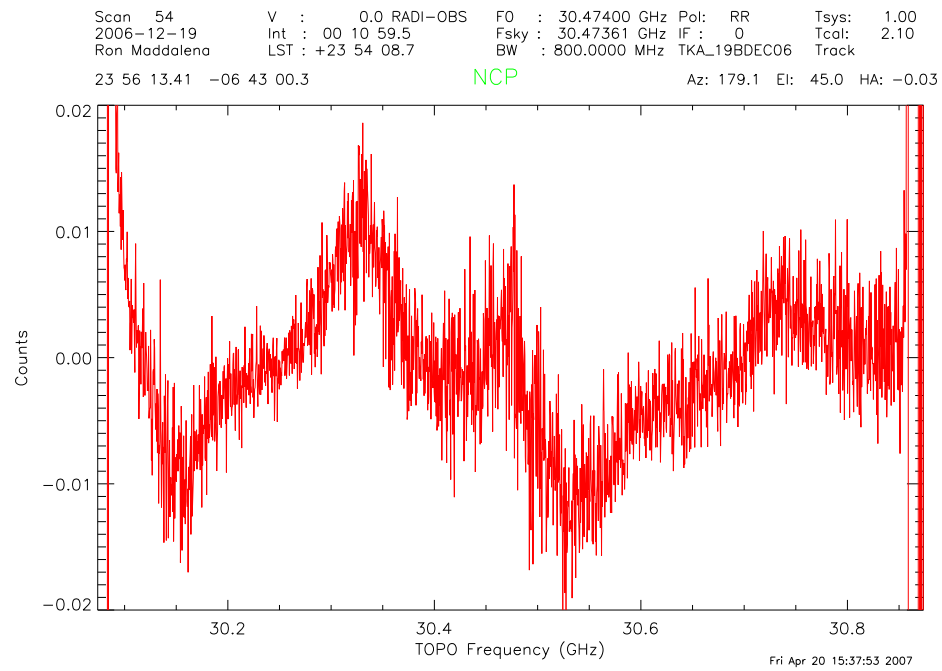

Fig. 2.— Combined NCP data from all four samplers (both feeds, both polarizations) with only the L diode firing and the phase-switch active.

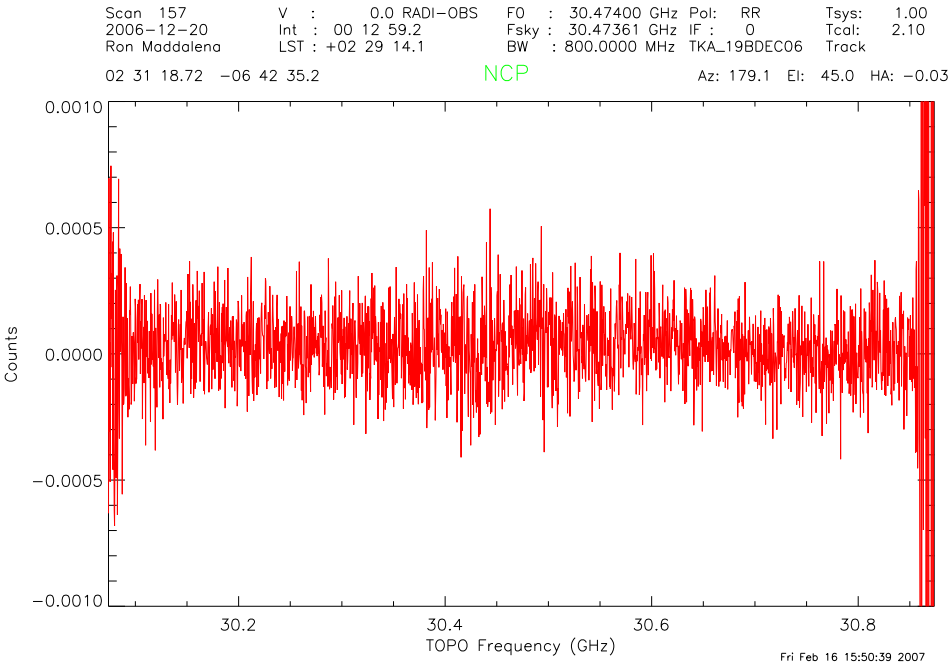

Fig. 3.— As in Figure 2, but with both diodes firing. Note that the scale for this figure is 5% of that in Figure 2.

as 9 seconds (3 seconds on, 3 seconds off, and 3 seconds moving) are possible by moving just the subreflector and may yield better baseline shapes. The resulting spectrum derived from this experimental subreflector-nodding mode is shown in Figure 5. This should be compared with standard slow-nodding in Figure 3.

The integration times for Figures 3 and 5 are different (and not actually represented in the displayed headers), so we can only consider the effect of the two observing modes on baseline shape not on the absolute noise in the spectrum. Using the ratio of the 600 MHz to 50 MHz noise again, it is 1.15 for the standard nod, but only 0.97 for the subreflector nod. The rapid nodding of the subreflector yields flatter baselines.

3.4. Cycle Times

How rapidly does the subreflector need to be nodded to produce flat baselines? When the cycle time is 9 seconds, the overhead for moving the subreflector is quite large, 33%. Since longer cycle times would still have only 3 seconds of overhead, the fractional overhead would be proportionally smaller. Slower nodding, however, will mean the gain changes could be larger. To check this we compared the final spectra for three different cycle times: 9 seconds, 36 seconds, and 288 seconds. The results are shown in Figures 5, 6, and 7. We have also examined the spectra for cycle times of 18 seconds, 72 seconds, and 144 seconds, but they are not shown here.

As the cycle time is increased from 9 seconds to 288 seconds (4.8 minutes), the noise in the spectra gets progressively worse; it is a factor of 2 worse for the 288 second cycles. The baseline quality also gets worse for long cycle times. It is obviously poor at 288 seconds (Figure 7), but appears to substantially degrade for cycle times longer than 36 seconds. Given the overhead to do a standard nod with a cycle time of 36 seconds, subreflector nodding is a more efficient observing mode. Furthermore, the data were taken under slightly better than median weather conditions. In worse weather, the faster cycle times possible with subreflector nodding should provide even better calibration than a standard slow nod.

4. System Temperatures

On February 21, 2007, during the daytime, we observed NGC 7027 to determine the T_{cal} and T_{sys} values for the Ka-band receiver. The results are shown in Figures 8- 11 (for T_{cal}) and Figures 12- 15 (for T_{sys}). NGC 7027 is a standard calibrator with a known flux of 5.23 Jy at 32 GHz (Ott et al., 1994, A&A, 284, 331). It has a size of $6''$, so this flux was corrected, assuming a Gaussian source distribution, using the method of Baars et al. (1973, IEEE Trans Antennas Propagat, Vol. AP-21, 461). Since the beamsize of the GBT varies significantly across Ka-band, the beam correction factor is frequency dependent and ranges from 1.12 at 26 GHz to 1.28 at 40 GHz.

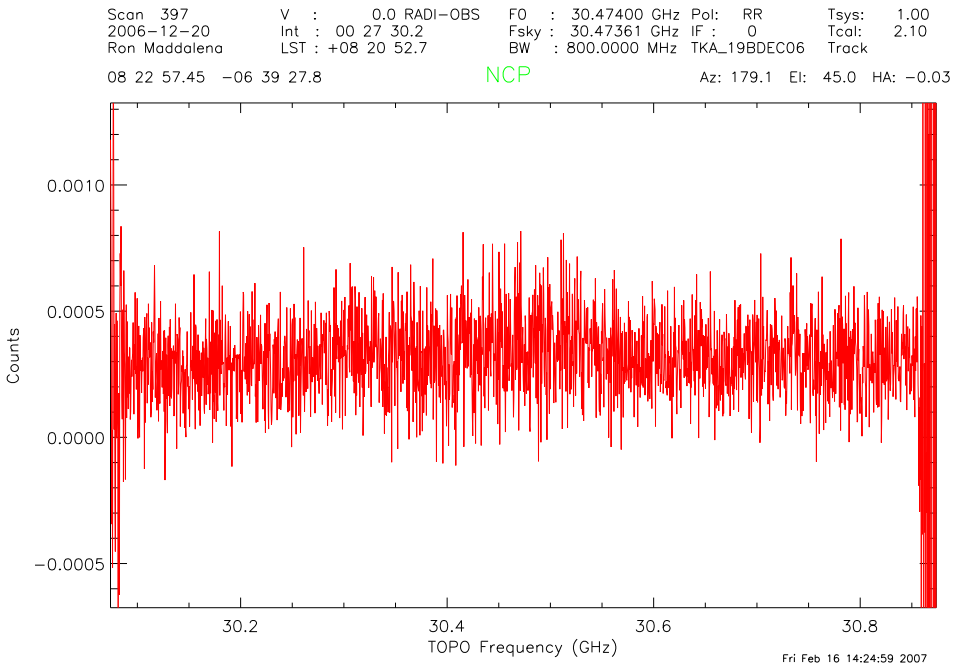

Fig. 4.— As in Figure 3, but with the phase-switch off; treating the receiver as a total power receiver.

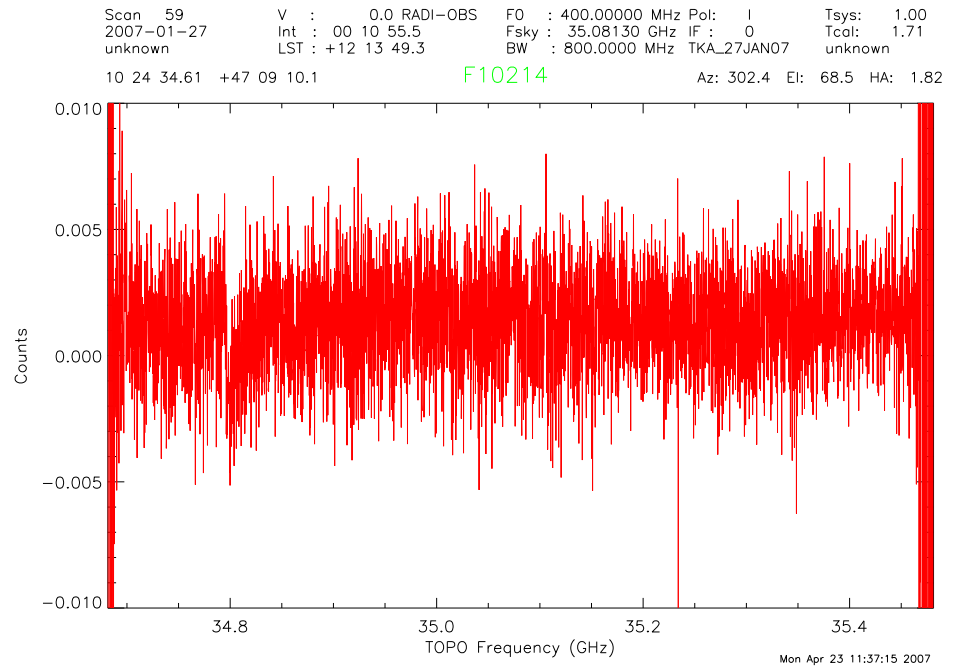

Fig. 5.— Observations of F10214 taken while nodding the subreflector. The L diode is firing and the phase switch is on. Data from all four samplers are combined, but only for the L polarization (since that is the only polarization with the noise diode firing).

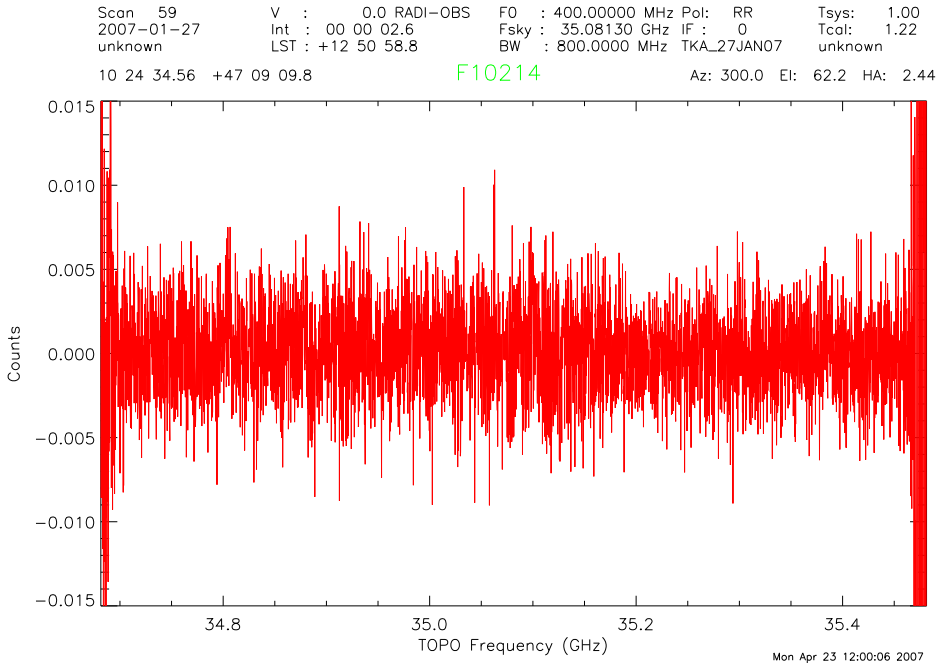

Fig. 6.— As in Figure 5, but a 36 second cycle time is simulated.

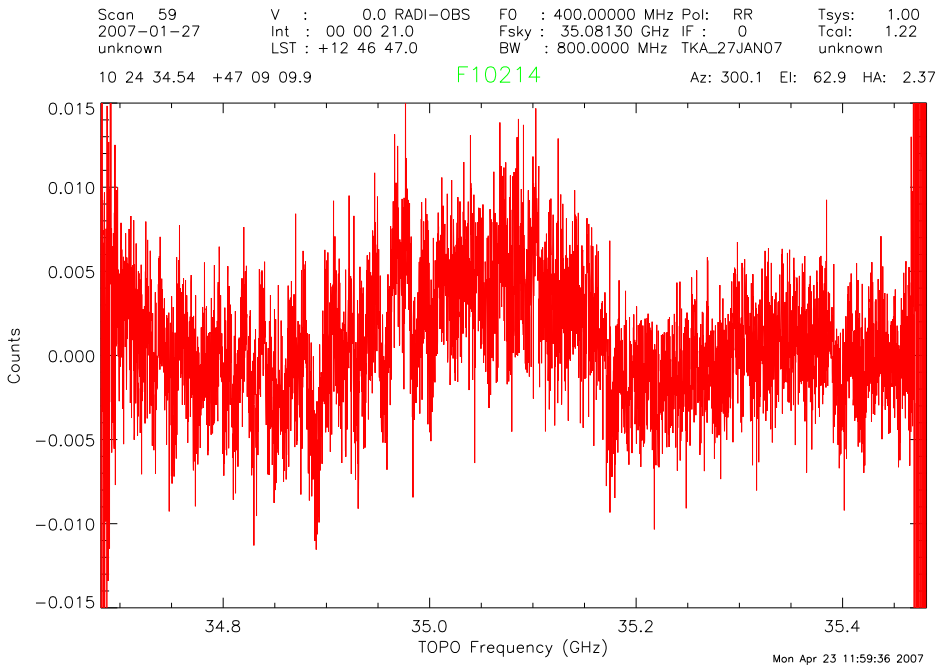

Fig. 7.— As in Figure 5, but a 4.8 minute cycle time is simulated.

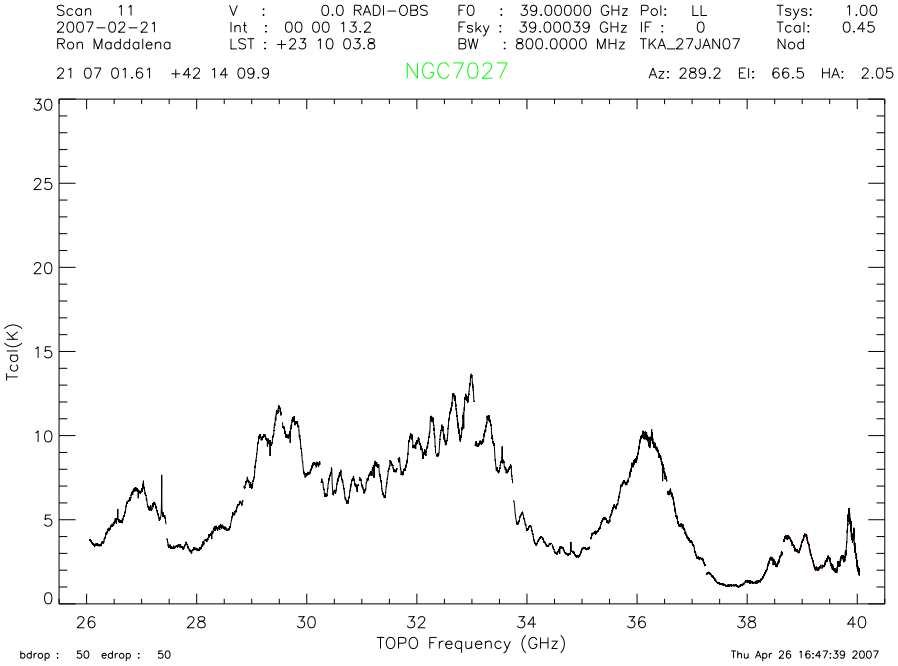

Fig. 8.— T_{cal} for Feed 2, R polarization.

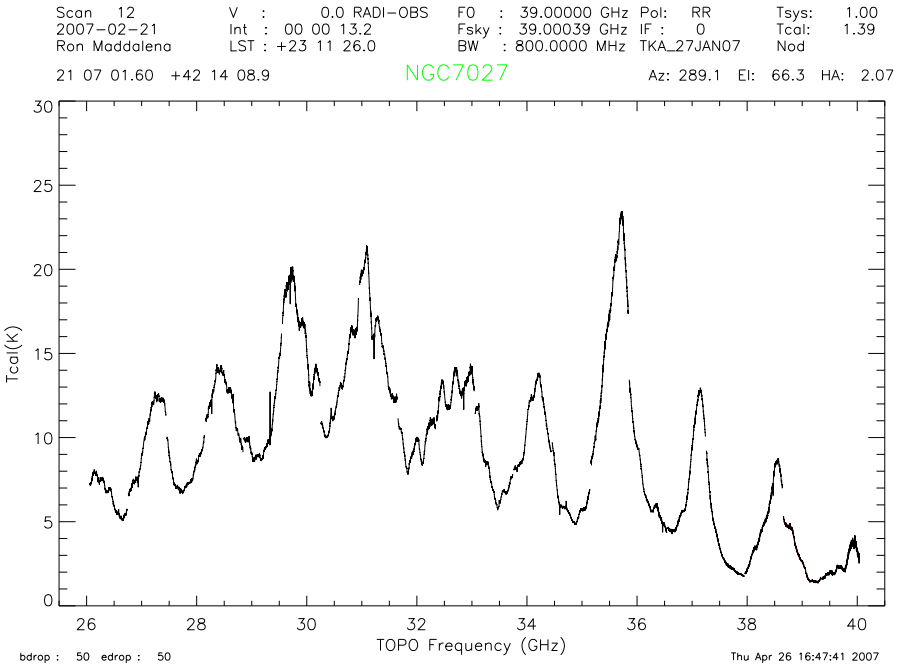

Fig. 9.— Same as in Figure 8, but for Feed 1, L polarization

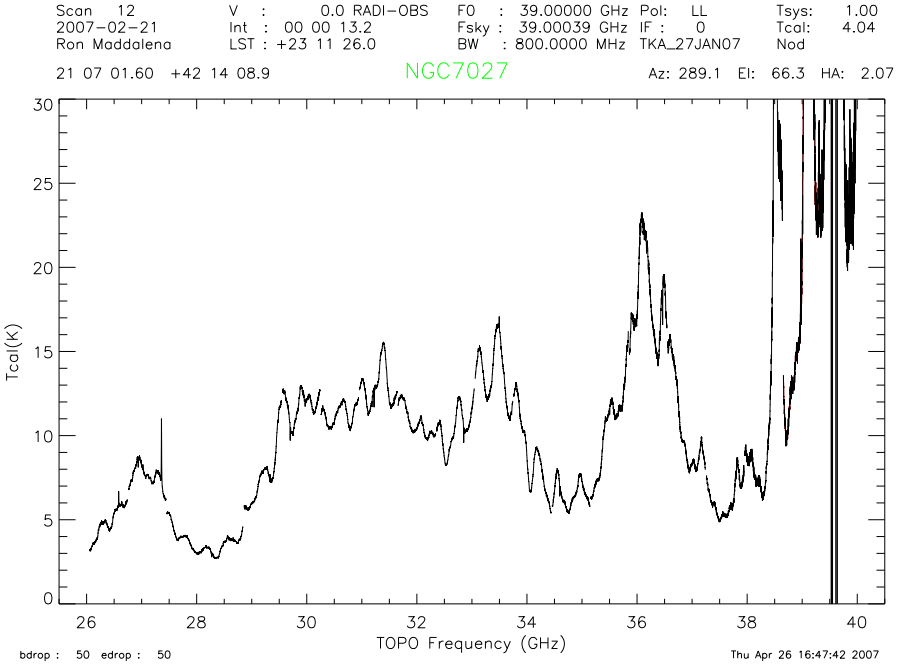

Fig. 10.— Same as in Figure 8, but for Feed 1, R polarization

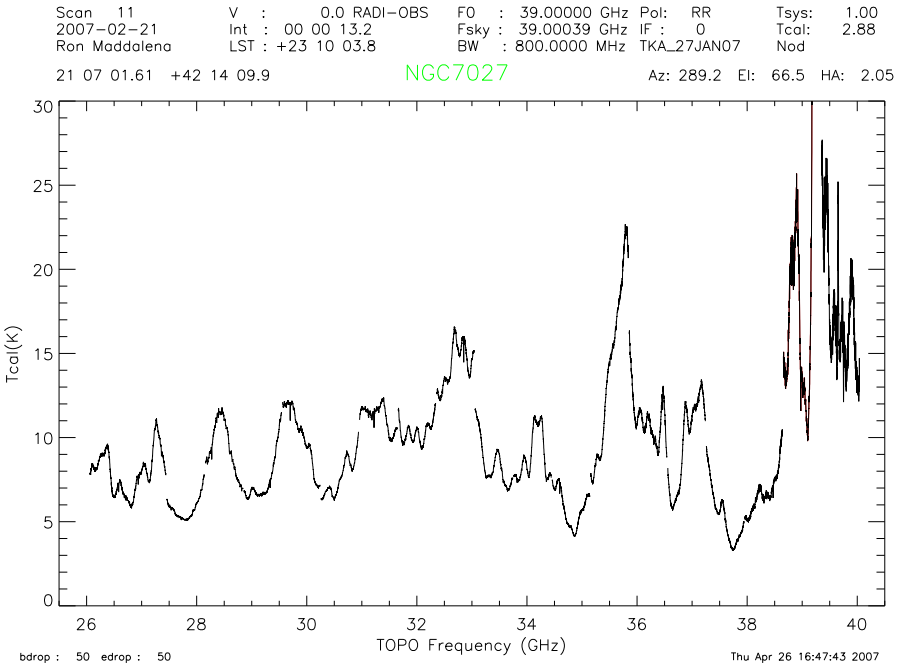

Fig. 11.— Same as in Figure 8, but for Feed 2, L polarization

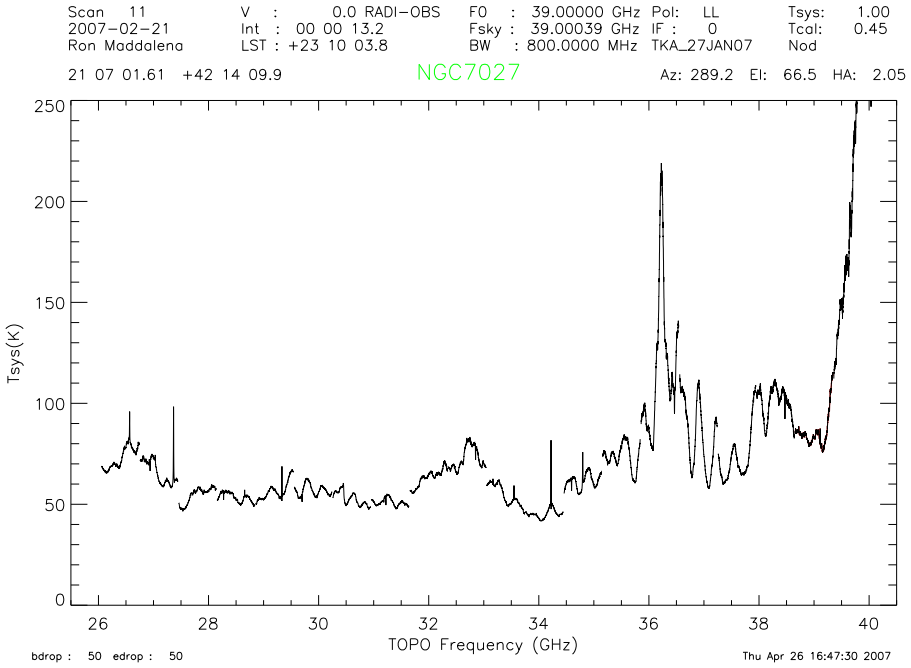

Fig. 12.— T_{sys} for Feed 2, R polarization.

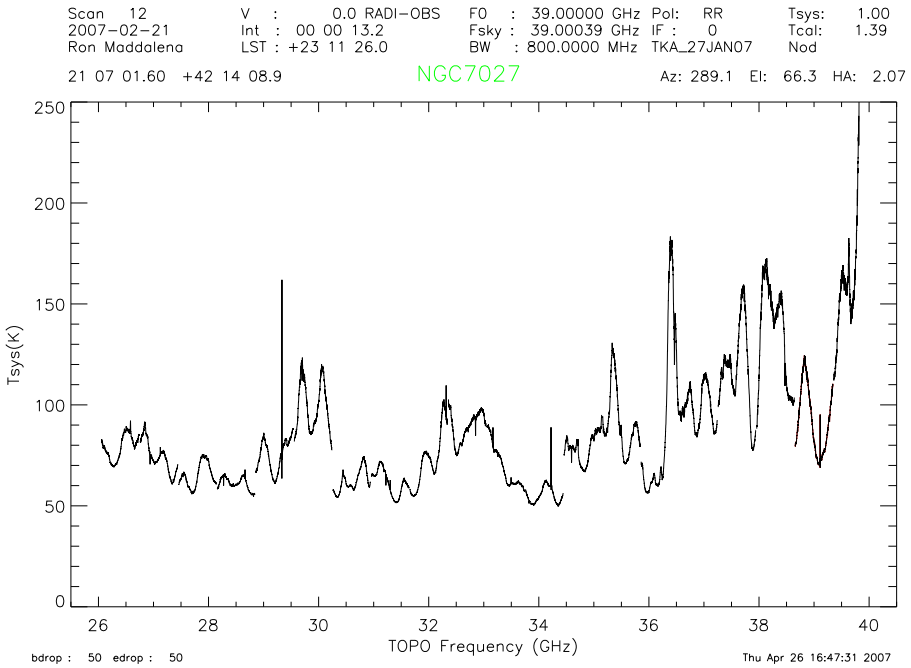

Fig. 13.— Same as in Figure 12, but for Feed 1, L polarization

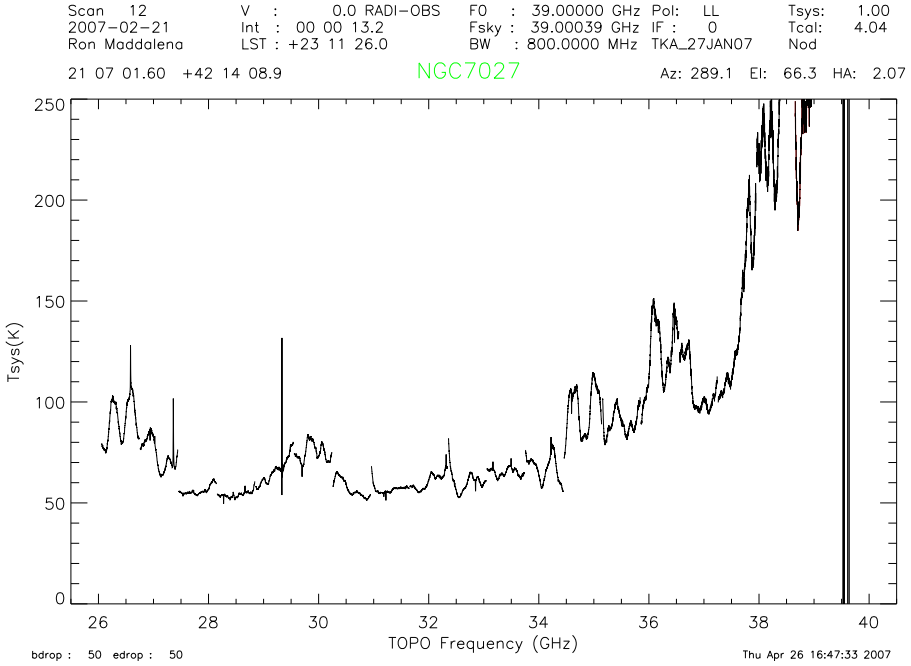

Fig. 14.— Same as in Figure 12, but for Feed 1, R polarization

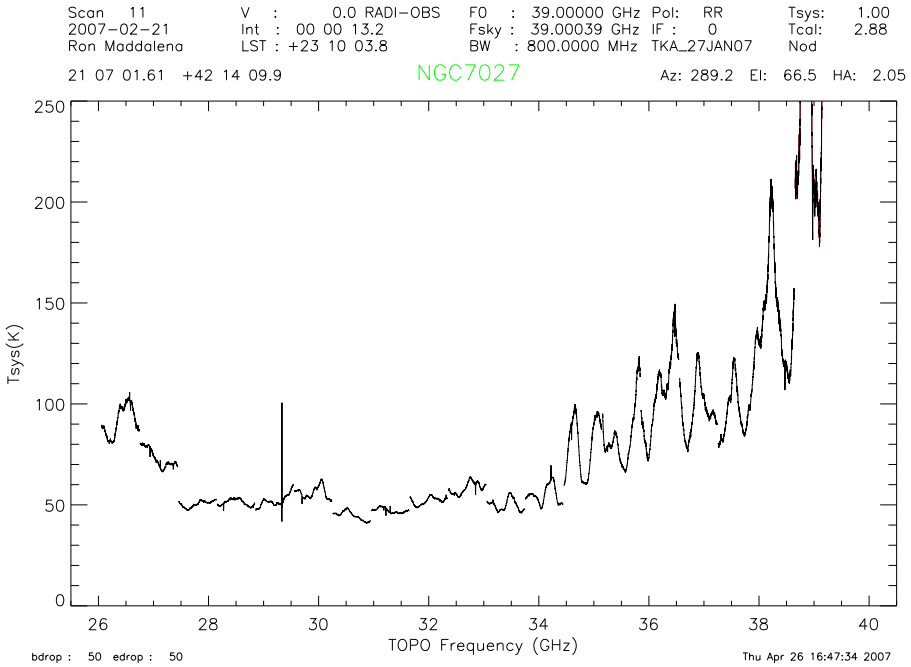

Fig. 15.— Same as in Figure 12, but for Feed 2, L polarization

The T_{cal} values range between 1-30 K depending on the frequency, polarization, and feed used for the observation. T_{sys} values range from 50-100 K across most of the band and from 100 K to over 250 K above 36 GHz. There are large oscillations in both T_{cal} and T_{sys} over relatively small frequency ranges. The use of scalar values of T_{cal} or T_{sys} in a calibration algorithm will not remove some significant baseline shapes due to the frequency structure in these quantities. Using a vector T_{cal} or T_{sys} should remove some baseline structures. These values also illustrate that the Ka-band receiver performs poorly above 36 GHz.

5. Astronomical Results

As an astronomical demonstration of the improved calibration algorithm and observing techniques, we observed the high redshift galaxy F10214 from the accepted GBT proposal of vanden Bout, Solomon, and Maddalena (GBT 05A-029). Observations on April 7, 2007 were made while firing both diodes, with the phase switches active, and nodding the subreflector. Observations on January 27, 2007 were made using the same configuration except only the L diode was firing. The effective integration time was 51 minutes in April and 22 minutes in January. We combined the data from both nights after calibration. The weather was slightly better than the median conditions on both nights.

Figure 16 shows the combined data from January and April, for an effective integration time of 73 minutes, over the entire 800 MHz bandwidth at 0.39 MHz frequency resolution. The spectrum has been shifted so that its mean is zero, but no other baseline has been fit to the data. The strong negative feature at 34.8 GHz is present in only the R polarization data. It is also visible in the T_{cal} and T_{sys} values (Figures 8-15). Therefore, this feature is certainly internal to the signal path.

Figure 17 shows our $\sim 3\sigma$ (peak) detection of CO(1-0) in F10214 using the Ka-band receiver on the GBT. These data have been boxcar smoothed to a resolution of 3.9 MHz, and has had a fifth order baseline fit to the results. Only the central 600 MHz of the spectrum are shown (the same region over which the baseline was fit). This galaxy has previously been detected in higher order transitions of CO and in HCN (see Solomon & vanden Bout, 2005, ARA&A, 43, 677 for a review). The redshift, peak flux, and linewidth all agree with the expectations from published values. The baselines are clearly flat enough to enable broad-line sources to be detected with the Ka-band receiver. The noise in this spectrum also matches expectations from the radiometer equation demonstrating the ability of this receiver to detect faint sources.

6. Outstanding Issues and Future Plans

All of the results described in this memo have come from using the Ka-band receiver as a total power receiver and not as a correlation receiver. Even when the phase-switches are being used, the data for each state have been treated separately. We have not addressed the outstanding issues

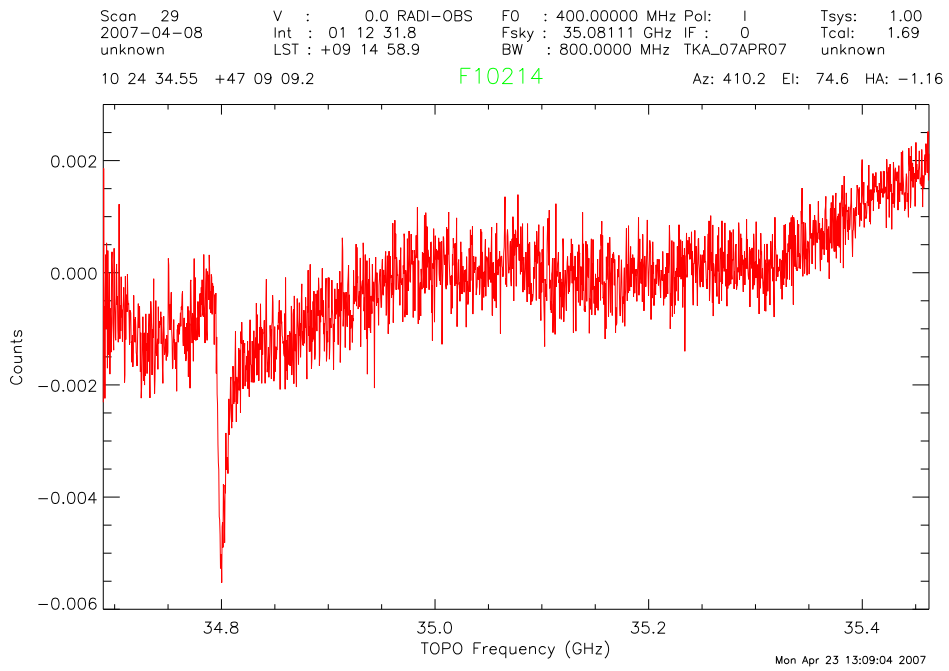

Fig. 16.— CO(1-0) spectrum of the z=2.3 galaxy F10214.

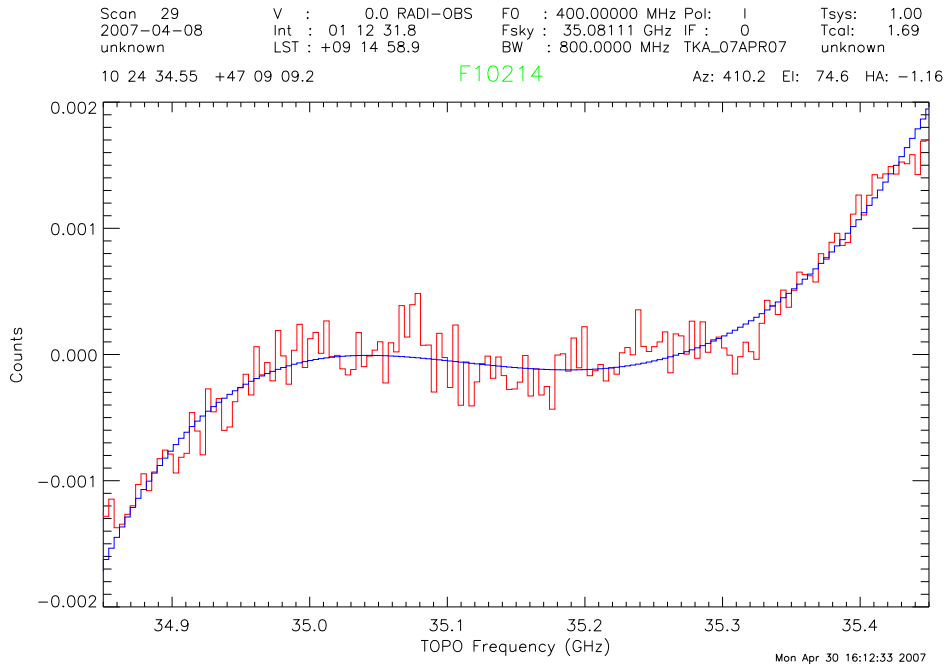

Fig. 17.— CO(1-0) spectrum of the z=2.3 galaxy F10214 after boxcar smoothing to 3.9 MHz resolution with a 5th order baseline shown in blue.

with the Zpectrometer tests.

Another major concern with the Ka-band receiver are the large variations (factors of two) in T_{cal} and T_{sys} over a few hundred MHz. Fortunately, this structure is fairly stable, and can be calibrated, so it does not appear to result in significant residual baseline structure. On top of this is the dramatic rise in T_{sys} above 35-36 GHz. T_{sys} values vary more dramatically with frequency above about 35 GHz, and are prohibitively high ($\gtrsim$120-150 K) above 36 GHz. T_{sys} across Ka-band is generally higher than one would expect from a traditional, non-correlation receiver. Improvements in the values and structure of T_{sys} and in the high frequency cutoff of the Ka-band receiver would be highly beneficial. Hopefully, the engineering work on the receiver during the summer shutdown will rectify these problems.

There are a few additional items that will need to be implemented or corrected to simplify the future use of the Ka-band receiver. First, subreflector nodding will need to be implemented as a standard observing mode in Astrid. Second, GBTIDL and SDFITS will need to be updated to accommodate the calibration algorithm including using vector T_{sys} and T_{cal} values. In addition, the IF cables are currently labeled incorrectly and the mm-wave converter and LO setting are not correct above 36 GHz. These issues will be addressed in the near future.

Thanks to all who have worked on the Ka receiver and its commissioning, especially Galen Watts, Roger Norrod, Larry Morgan, Brian Mason, and Jules Harnett. Special thanks to Paul vanden Bout and Phil Solomon for permission to observe a galaxy from their proposal.